Manufacturing Letters 28 (2021) 35–41

Contents lists available at ScienceDirect

Manufacturing Letters

journal homepage: www.elsevier.com/locate/mfglet

Letters

Biologically-inspired rib designs for captured powder damping in additive manufacturing

Michael Gomez [a,b], Gregory Corson [a], Eric Heikkenen [a], Kevin Sisco [a], Michael Haines [a], Tony Schmitz [a,b,*]

[a] University of Tennessee, Knoxville, 1512 Middle Dr., Knoxville, TN 37996, USA
[b] Manufacturing Science Division, Oak Ridge National Laboratory, Oak Ridge, TN 37830, USA

ARTICLE INFO

Article history:
Received 25 January 2021
Accepted 3 March 2021
Available online 24 March 2021

Keywords:
Damping
Powder
Additive manufacturing
Structural dynamics

ABSTRACT

This paper describes the design and impact testing of laser powder bed fusion 316L stainless steel walls with captured powder cores. The purpose is to determine the effect of biologically-inspired internal ribs on the mode shapes and damping ratios. Comparison is made between five designs: solid and powder core with {no ribs, vertical ribs, hatched ribs, and bat wing ribs}. The powder core increases damping ratios by factors of 2 to 58 depending on the mode number and design. Mode shape and modal parameter evaluations show that the ribbed powder core designs enable tailored dynamics relative to the solid wall.

1. Introduction

As discussed by Helms *et al.*, "Biologically inspired engineering design uses analogies to biological systems to develop solutions for engineering problems" [1]. In this study, we mimic biological bone structures to add internal stiffening features, or ribs, to captured powder cavities within metal walls produced by powder fusion (PBF). As shown in prior work, the retention of unsolidified powder within otherwise solid PBF structures increases damping, or energy dissipation, to improve dynamic performance [2–8].

As demonstrated in [3], the presence of captured powder cores within stainless steel walls (clamped-free-free-free boundary conditions) increased damping substantially. It was reported that the viscous damping ratio increased by one to two orders of magnitude for captured powder designs over a solid wall of the same external dimensions and boundary conditions, depending on the internal powder core width and mode number (the first three bending modes were analyzed). However, it was also observed that the mode shapes were distorted due to the hollow core.

In this work, we modify the captured powder cavity design to include biologically-inspired, solidified ribs that separate the individual powder cores. The intent is to retain the advantage of increased damping through captured powder while adding stiffness through the rib placement. Three biologically-inspired designs are considered: 1) radial ribs based on the bat wing (Fig. 1, left) [9]; 2) parallel, unidirectional ribs similar to the human thoracic cage (Fig. 1, right) [10]; and 3) a hatched design with vertical and horizontal superposition of the parallel human rib structure. The wall and rib geometry dimensions are displayed in Fig. 2. In each case, the 2 mm powder cores are centered within the 5 mm wall thickness and the rib cross-sectional dimensions are 1 mm wide by 5 mm thick.

2. Material and methods

All five walls were manufactured using a Farsoon FS271M PBF printer with a 500 W Yb fiber laser. The powder was 316L stainless steel with a nominally spherical shape and manufacturer-specified 15 μm to 45 μm size range; the particle size distribution was not provided. A raster-in-stripes scan strategy with a 10 mm stripe width was selected for printing. The layer height was 41 μm as the walls were printed from the foundation to the top as seen in Fig. 2. The processing parameters are listed in Table 1.

3. Measurement procedure

To quantify the wall structural dynamics, impact testing was performed on the five designs: solid, 2 mm powder core (no internal ribs), vertical ribs, hatched ribs, and bat wing ribs. For the latter three biologically-inspired designs, the 2 mm powder cores were separated by the solid internal ribs. To perform the impact testing, a small hammer (PCB model 086E80) was used to excite the wall and a low-mass accelerometer (PCB model 352C23) was used to measure the vibration response. MLI's MetalMax TXF software

* Corresponding author.

https://doi.org/10.1016/j.mfglet.2021.03.002

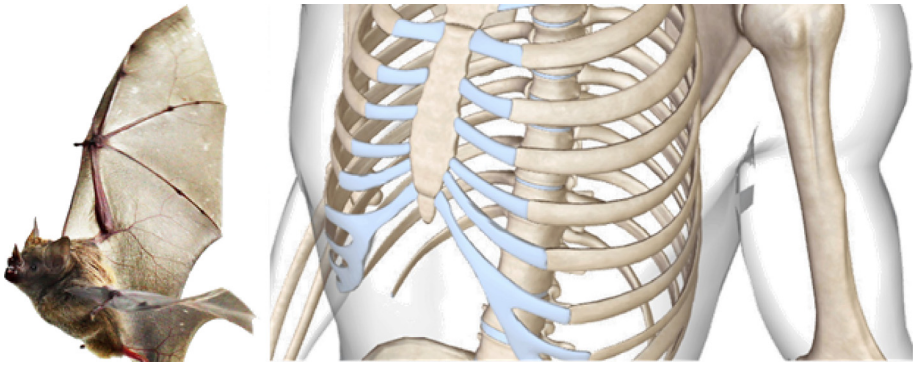

Fig. 1. Biological inspiration for solidified ribs within captured powder cores for PBF structures. (Left) bat wing with radial features extending from the elbow and wrist side [9]; and (right) parallel structure for the human thoracic cage [10].

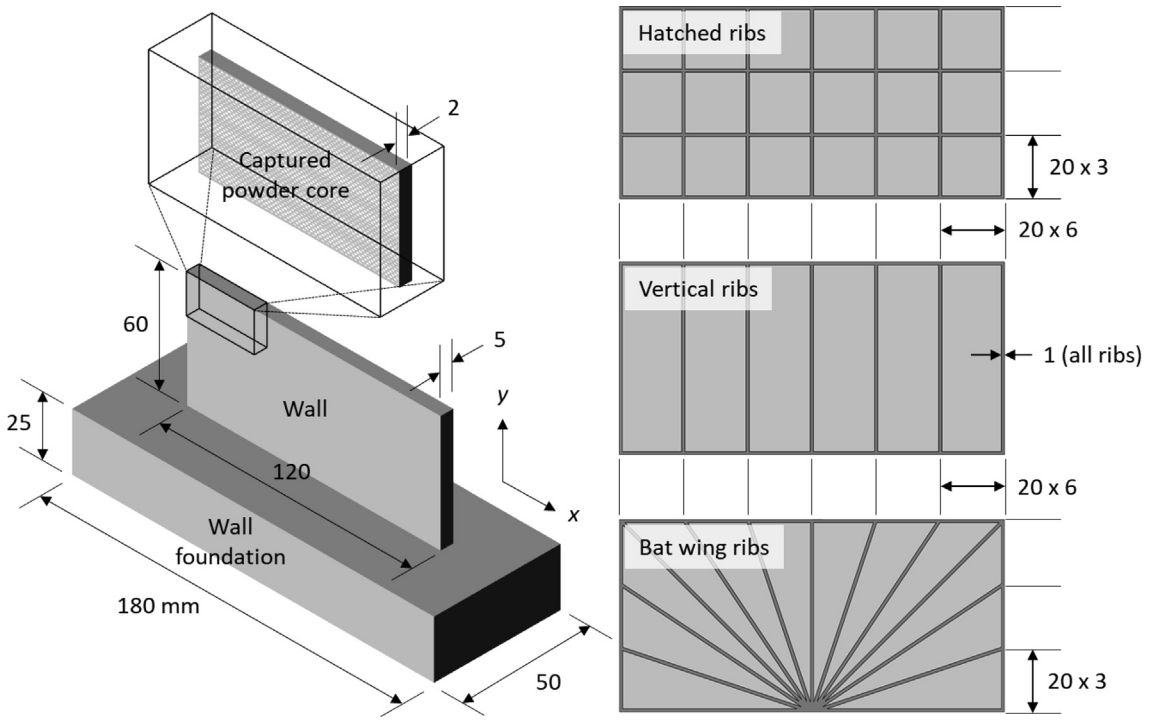

Fig. 2. Wall designs with solidified ribs and captured powder cores between the ribs.

Table 1
Laser PBF processing parameters.

Laser power (W)	Scan velocity (mm/s)	Hatch size (μm)	Laser spot size (μm)	Preheat temperature (deg C)
240	1000	70	93	100

was used for data acquisition and frequency response function, FRF, calculation. Measurements were performed over a grid of points spaced at 10 mm intervals in both the horizontal and vertical directions; the 78 locations for the 6 × 13 grid are shown in Fig. 3.

A direct FRF, where the impact force input is applied at the accelerometer location, was measured at the top left corner. For the cross FRFs, the accelerometer was located at the top left corner, but the force was applied at the 77 remaining grid locations. The direct FRF for each wall was used to identify the natural frequency, modal stiffness, and (dimensionless) modal viscous damping ratio for the first three modes. The direct and cross FRFs for each wall were used to define the first three mode shapes [11].

4. Results and discussion

The natural frequency, f_n, modal stiffness, k, and modal viscous damping ratio, ζ, for the first three modes of all five walls are listed

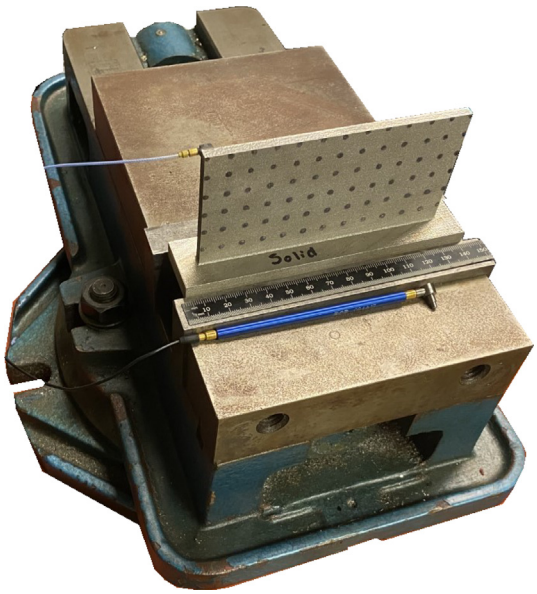

Fig. 3. Experimental setup. Each wall was clamped in a vise to constrain the wall foundation. The accelerometer was attached to the back side of the wall's top left corner and the impact hammer was used to excite the wall at the 78 front side locations. The 152 mm steel ruler provides scale.

in Table 2. The modal parameters were identified by the peak-picking approach applied to the real and imaginary parts of the complex-valued direct FRFs [11]. It is seen that the natural frequencies are significantly lower for the 2 mm core and bat wing ribs designs. The vertical ribs and hatched ribs walls, on the other hand, have natural frequencies that exceed the solid wall values for all three modes. This is a combination of the rib stiffness and reduced distributed mass from the lower-density powder cores.

Interestingly, the vertical and hatched rib designs offer comparable modal stiffness values to the solid wall with lower volumes of solid metal. The vertical ribs wall has a solidified cross-sectional area (i.e., the two-dimensional view in Fig. 2) of 636 mm^2 for the ribbed portion; this is only 8.8% of the solid wall cross-sectional area (7200 mm^2). Including the front and back solid faces that bracket the 2 mm powder cores, the solidified volume for the vertical ribs wall is 22872 mm^3, or 63.5% of the solid wall volume (36000 mm^3). The hatched rib wall has a cross-sectional area of 852 mm^2 for the ribbed portion, which is 11.8% of the solid wall area. The total solidified volume for the hatched ribs wall is 23304 mm^3, or 64.7% of the solid wall volume.

Table 2 also shows that the damping increases substantially with the presence of the powder cores. To enable a visual comparison of the damping increase, the damping ratios for the four powder core designs were normalized to the solid wall damping ratios for all three modes; see Fig. 4. To interpret the figure, the vertical

Table 2
Modal parameters for first three modes of five wall designs.

Modal parameter	Solid wall			2 mm core wall			Vertical ribs wall		
	Mode 1	Mode 2	Mode 3	Mode 1	Mode 2	Mode 3	Mode 1	Mode 2	Mode 3
f_n (Hz)	968	1581	3079	535	1296	1921	1015	1707	3212
$k \times 10^6$(N/m)	3.4	3.4	12.4	1.4	3.7	9.3	4.0	2.8	11.7
ζ (%)	0.45	0.19	0.33	3.9	2.3	2.8	6.0	11.0	6.8
	Hatched ribs wall			**Bat wing ribs wall**					
f_n (Hz)	1017	1673	3318	583	1334	2100			
$k \times 10^6$(N/m)	3.3	2.8	10.1	2.0	4.4	12.6			
ζ (%)	6.8	9.9	8.3	0.91	2.1	2.0			

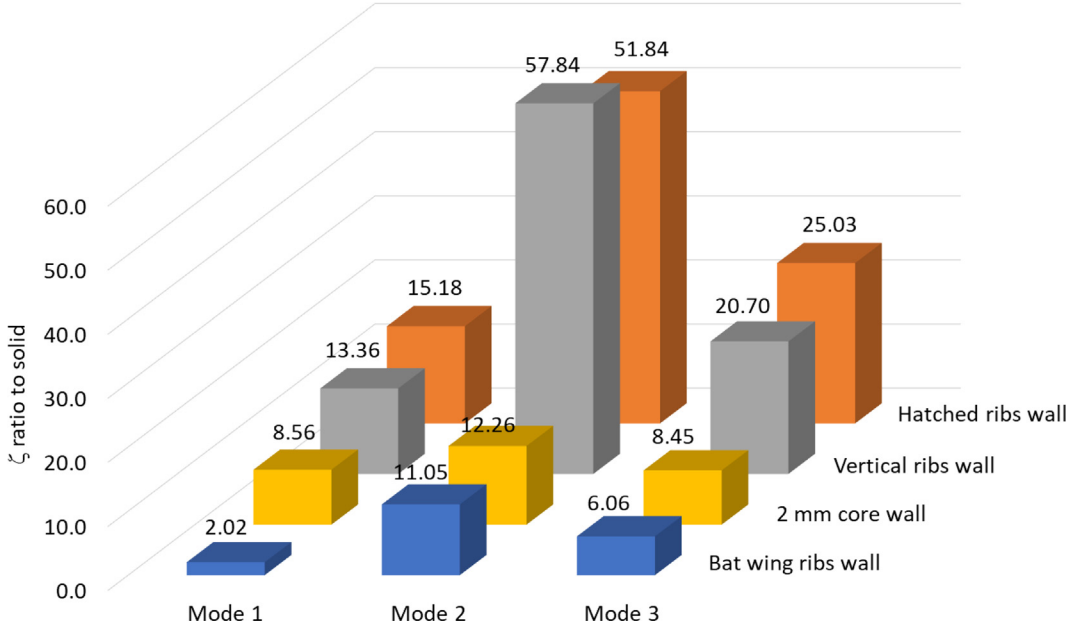

Fig. 4. Ratio of powder core design damping to the solid wall damping for the first three bending modes.

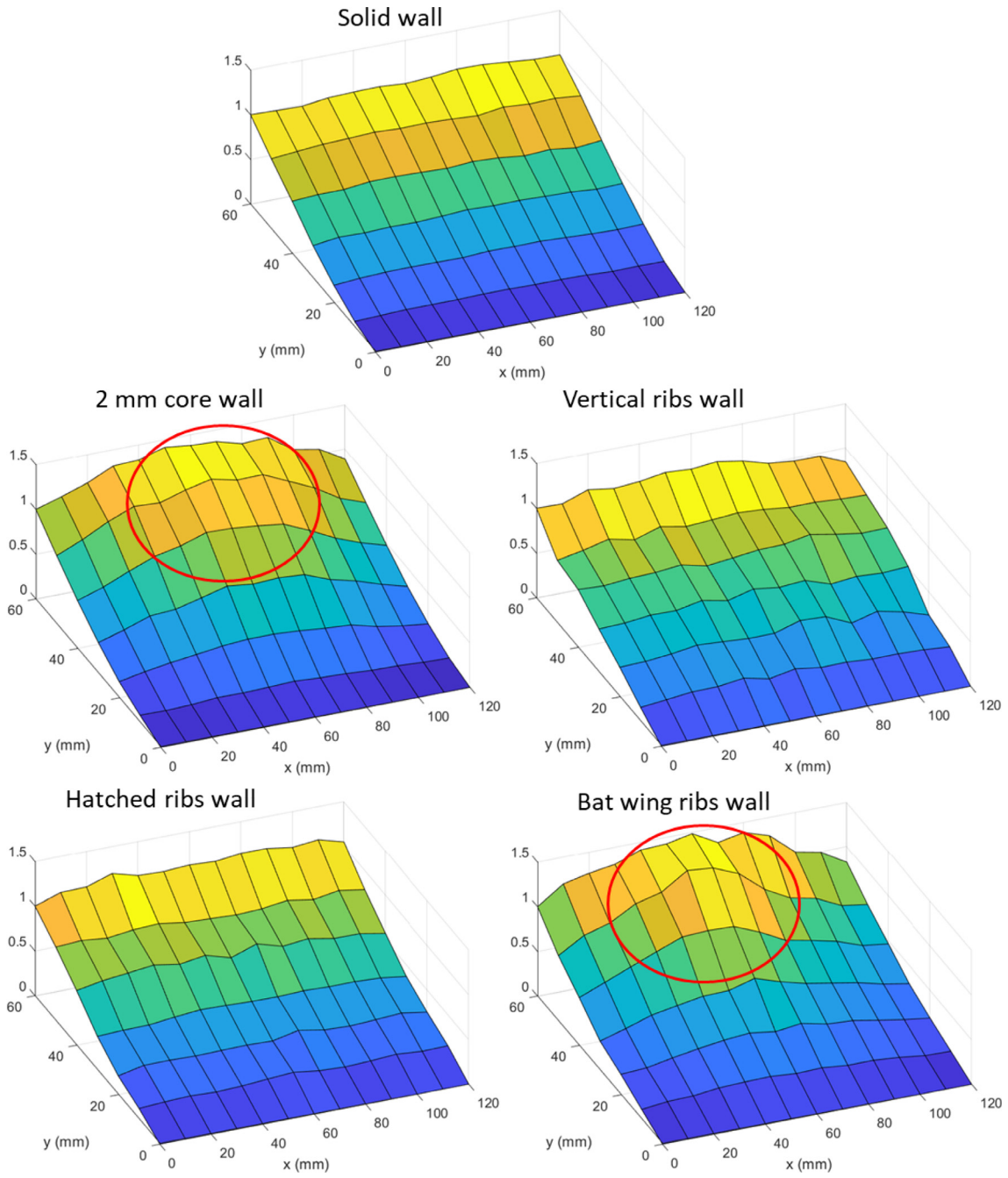

Fig. 5. First mode shape for five wall designs. The mode shape distortion at the top center of the 2 mm core and bat wing designs is highlighted by the red ovals. (For interpretation of the references to colour in this figure legend, the reader is referred to the web version of this article.)

ribs wall first mode ζ value is 13.36 times higher than the first mode ζ value for the solid wall, for example.

The measured mode shapes are displayed in Figs. 5-7. For mode 1 in Fig. 5, it is observed that the 2 mm core and bat wing designs both exhibit distortion (relative to the solid wall mode shape) near the top center span of the clamped-free-free-free wall. This result is not surprising for the biologically-inspired bat wing design since the thrust and lift during bat flight depends on compliant wing deformation during the flapping motion [12–13]. A similar result is seen for mode 2 (Fig. 6). In this case, the distortion occurs at two locations which are mirrored about the vertical centerline with opposite directions. Fig. 7 displays the third mode shapes. Here, the 2 mm core and bat wing design mode shapes again demonstrate distortion relative to the solid wall, but the location

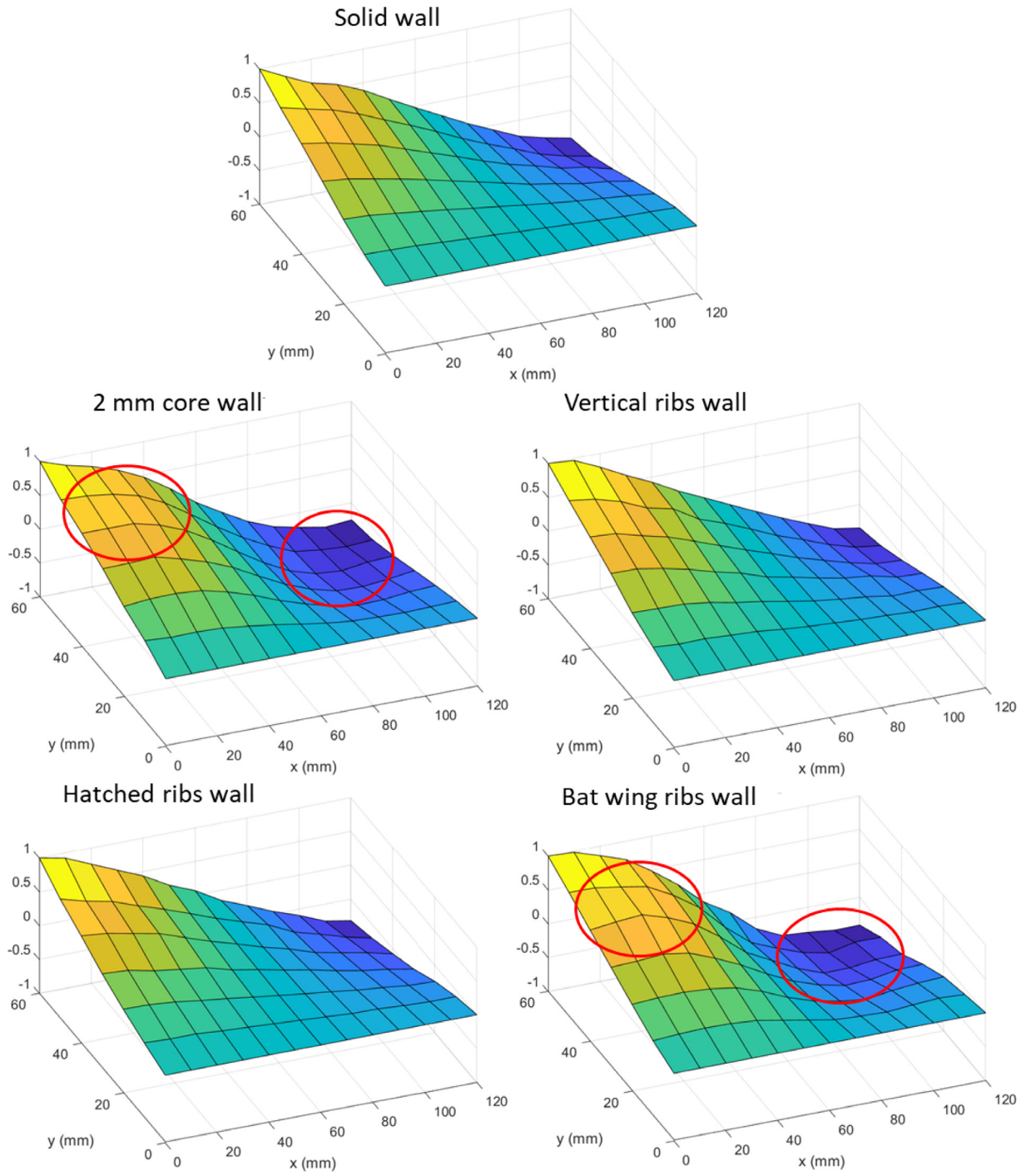

Fig. 6. Second mode shape for five wall designs. The mirrored distortions of the 2 mm core and bat wing designs are highlighted by the red ovals. (For interpretation of the references to colour in this figure legend, the reader is referred to the web version of this article.)

for maximum distortion is nearer the wall foundation for the 2 mm core than the bat wing design. This is because the bat wing ribs all meet at the bottom center of the wall (i.e., the bat's wrist) and stiffen the wall locally.

Since mode shapes are not inherently scaled, standard practice is to normalize all measurement results using the direct FRF measurement. This provides a value of 1 at the direct FRF location and scaled values (relative to the direct FRF amplitude) at all cross FRF

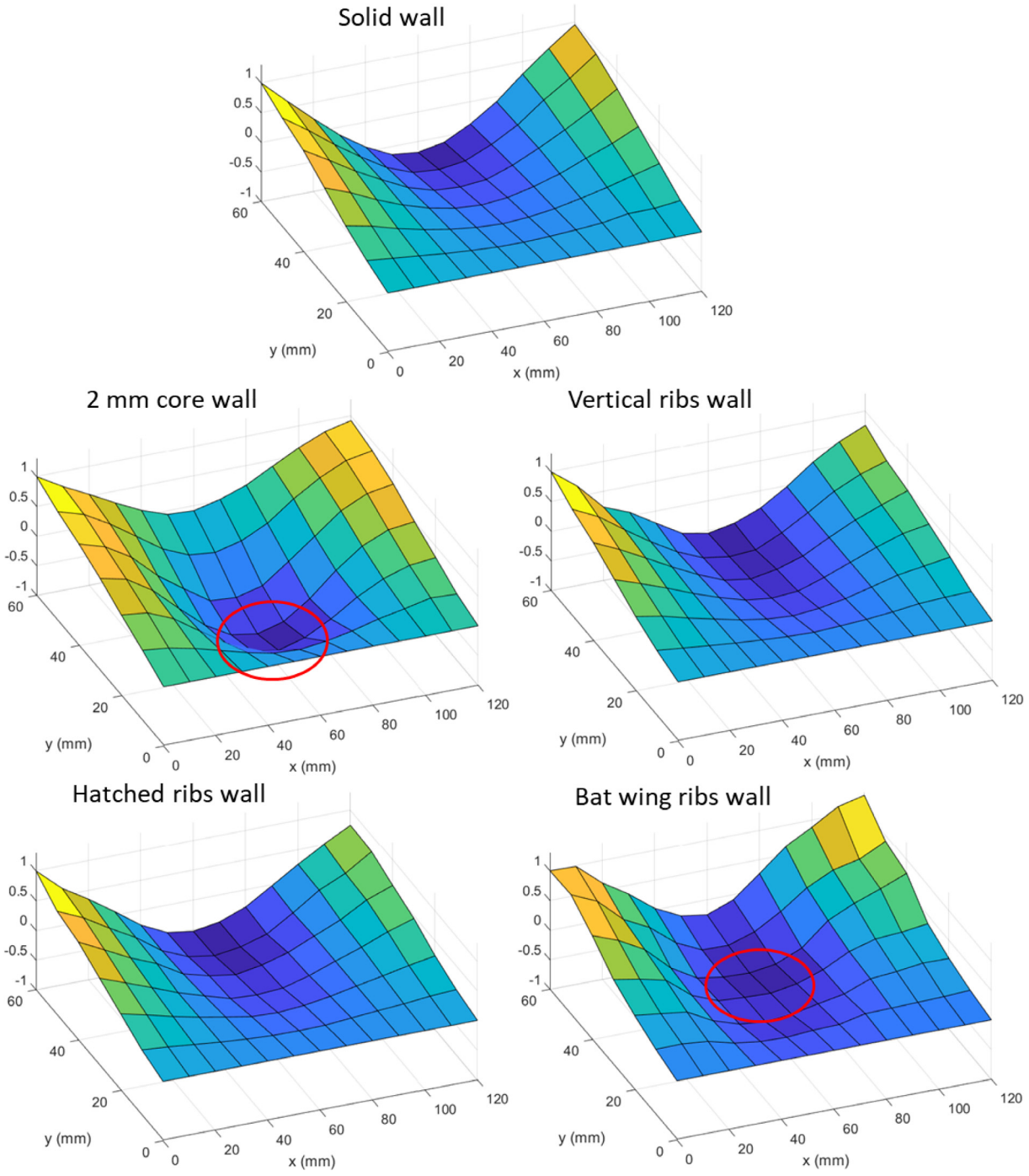

Fig. 7. Third mode shape for five wall designs. The mode shape distortions for the 2 mm core and bat wing designs are highlighted by the red ovals. The locations of maximum distortion differ due to the higher stiffness where the bat wing ribs meet at the bottom center of the wall. (For interpretation of the references to colour in this figure legend, the reader is referred to the web version of this article.)

locations. This approach was applied in each panel of Figs. 5-7. As a final comparison, the captured powder wall mode shapes were instead normalized to the solid wall mode shapes. In this case, the mode shapes indicate the motion amplitude relative to the solid wall. The results for mode 3 are presented in Fig. 8. Because the maximum value for all points on all mode shapes is 0.25 or less, this demonstrates that the captured powder designs offer higher dynamic stiffness (i.e., the product of stiffness and damping) than the solid wall. The local distortion in the 2 mm core and bat wing ribs walls is again observed.

In summary, it is observed that: 1) the added ribs strongly influence the wall mode shapes without sacrificing the increased damping made possible by the captured powder; and 2) the biologically-inspired designs mimic their function in nature. Specifically, the bat wing enables flapping motion by location-dependent distortion and higher stiffness near the wrist (to enable

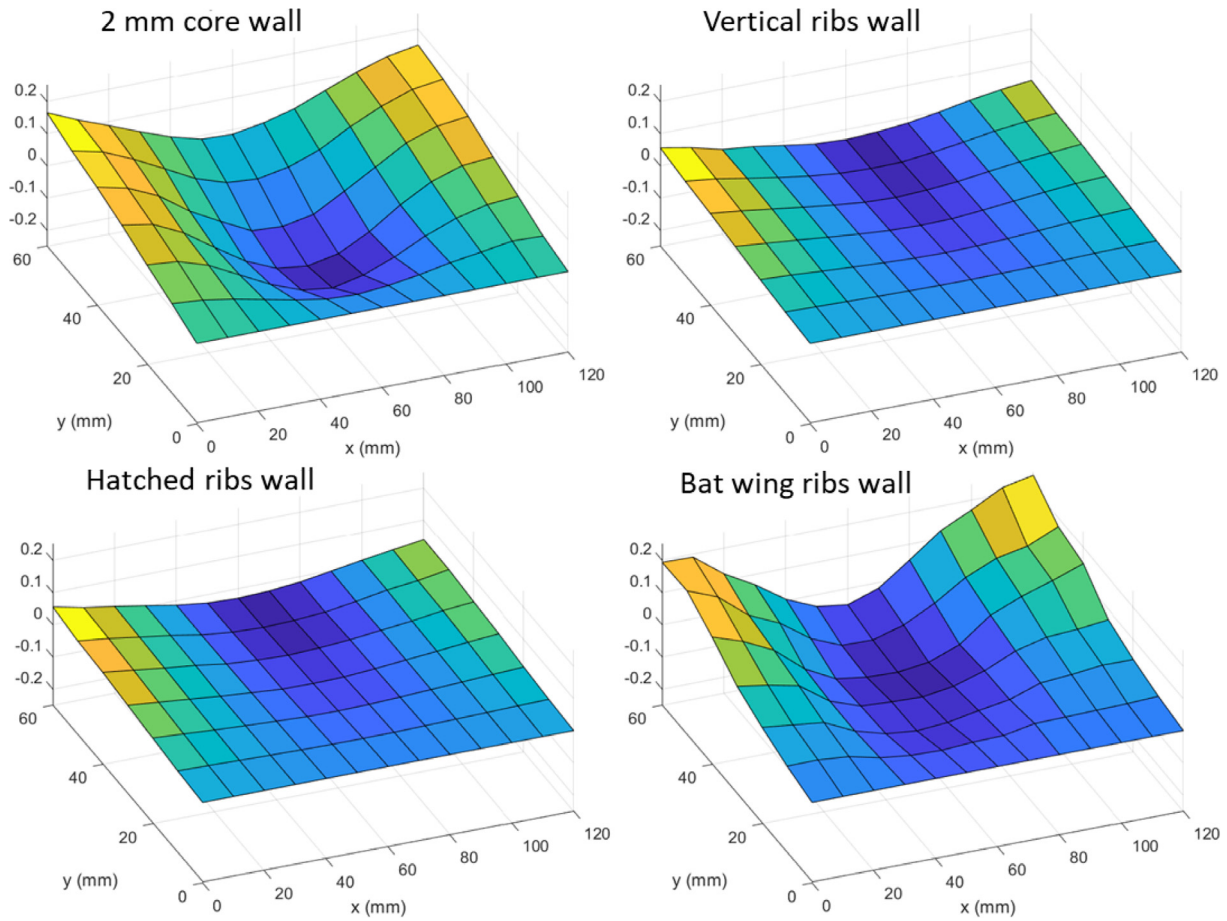

Fig. 8. Third mode shape for captured powder walls normalized to the solid wall direct FRF. Because all values are 0.25 or less, the captured powder walls offer increased dynamic stiffness over the solid wall.

force transfer), while the parallel thoracic cage minimizes distortion approximately uniformly to protect the internal organs.

Declaration of Competing Interest

The authors declare that they have no known competing financial interests or personal relationships that could have appeared to influence the work reported in this paper.

Acknowledgements

This research was supported by the DOE Office of Energy Efficiency and Renewable Energy (EERE), Manufacturing Science Division, and used resources at the Manufacturing Demonstration Facility, a DOE-EERE User Facility at Oak Ridge National Laboratory.

References

[1] Helms M, Vattam SS, Goel AK. Biologically inspired design: process and products. Des Stud 2009;30(5):606–22.
[2] Schmitz T, Betters E, West J. Increased damping through captured powder in additive manufacturing. Manuf Lett 2020;25:1–5.
[3] Schmitz T, Gomez M, Ray B, Heikkenen E, Sisco K, Haines M, et al. Damping and mode shape modification for additively manufactured walls with captured powder. Precis Eng 2020;66:110–24.
[4] Scott-Emuakpor OE, Beck J, Runyon B, George T. Multi-factor model for improving the design of damping in additively manufactured components. In: AIAA Scitech 2020 Forum. p. 1631.
[5] Scott-Emuakpor O, George T, Runyon B, Langley B, Sheridan L, Holycross C, et al. Forced-response verification of the inherent damping in additive manufactured specimens. In: Mechanics of additive and advanced manufacturing. Cham: Springer; 2019. p. 81–6. Volume 8.
[6] Scott-Emuakpor O, George T, Runyon B, Sheridan L, Holycross C, O'Hara R. Assessing manufacturing repeatability of inherently damped nickel alloy components via forced-response testing. Turbo expo: Power for land, sea, and air (Vol. 58677, p. V006T24A010). American Society of Mechanical Engineers; 2019.
[7] Scott-Emuakpor OE, George T, Beck J, Runyon BD, O'Hara R, Holycross C, et al. Inherent damping sustainability study on additively manufactured nickel-based alloys for critical part. In: AIAA Scitech 2019 Forum. p. 0410.
[8] Scott-Emuakpor, O., George, T., Runyon, B., Holycross, C., Langley, B., Sheridan, L., O'Hara, R., Johnson, P. and Beck, J., 2018, June. Investigating Damping Performance of Laser Powder Bed Fused Components With Unique Internal Structures. In Turbo Expo: Power for Land, Sea, and Air (Vol. 51159, p. V07CT35A020). American Society of Mechanical Engineers.
[9] https://phys.org/news/2019-09-biology-wings-lessons-cold-weather.html.
[10] https://dislocatedrib.org/first-rib-mobilization-self/.
[11] Schmitz T, Smith KS. Mechanical vibrations: modeling and measurement. Springer Science & Business Media; 2011.
[12] Gopalakrishnan P, Tafti DK. Effect of wing flexibility on lift and thrust production in flapping flight. AIAA J 2010;48(5):865–77.
[13] Hedenström A, Johansson LC, Wolf M, Von Busse R, Winter Y, Spedding GR. Bat flight generates complex aerodynamic tracks. Science 2007;316(5826):894–7.